Published in final edited form as:
Free Radic Biol Med. 2019 November 01; 143: 433–440. doi:10.1016/j.freeradbiomed.2019.08.027.

Covalent modification of phosphatidylethanolamine by 4-hydroxy-2-nonenal increases sodium permeability across phospholipid bilayer membranes

Olga Jovanović[a], **Sanja Škulj**[b], **Elena E. Pohl**[a,*], **Mario Vazdar**[b,**]

[a]Institute of Physiology, Pathophysiology and Biophysics, Department of Biomedical Sciences, University of Veterinary Medicine, Vienna, Austria

[b]Division of Organic Chemistry and Biochemistry, Rudjer Bošković Institute, Zagreb, Croatia

Abstract

Reactive aldehydes (RAs), such as 4-hydroxy-2-nonenal (HNE) and 4-oxo-2-nonenal (ONE), produced by cells under conditions of oxidative stress, were shown to react with phosphatidylethanolamine (PE) in biological and artificial membranes. They form RA-PE adducts, which affect the function of membrane proteins by modifying various biophysical properties of the membrane. The ratio of protein to lipid in biological membranes is different, but can reach 0.25 in the membranes of oligodendrocytes. However, the impact of RA-PE adducts on permeability (*P*) of the neat lipid phase and molecular mechanism of their action are poorly understood. In this study, we showed that HNE increased the membrane *P* for ions, and in particular for sodium. This effect depended on the presence of DOPE, and was not recorded for the more toxic compound, ONE. Molecular dynamics simulations suggested that HNE-PE and ONE-PE adducts anchored different positions in the lipid bilayer, and thus changed the membrane lipid area and bilayer thickness in different ways. Sodium permeability, calculated in the presence of double HNE-PE adducts, was increased by three to four orders of magnitude when compared to P_{Na} in adduct – free membranes. A novel mechanism by which HNE alters permeability of the lipid membrane may explain the multiple toxic or regulative effects of HNE on the function of excitable cells, such as neurons, cardiomyocytes and neurosensory cells under conditions of oxidative stress.

1 Introduction

Mitochondria convert oxygen and substrates into adenosine triphosphate (ATP) in the process of oxidative phosphorylation. During that process, small amounts of superoxide anion radicals ($O_2^{-}\cdot$) are formed due to incomplete reduction of molecular oxygen to water [1]. Superoxide anion radicals give rise to other reactive oxygen species (ROS) and lipid oxidation products as a consequence of peroxidation of polyunsaturated fatty acids (PUFAs) [2,3]. Various reactive aldehydes (RAs) are formed during a cascade of subsequent reactions [4]. The most common RA formed under conditions of oxidative stress is 4-hydroxy-2E-nonenal (HNE) [5]. It was reported that whereas cellular concentrations of HNE under

**Corresponding author. mario.vazdar@irb.hr (M. Vazdar). *Corresponding author. elena.pohl@vetmeduni.ac.at (E.E. Pohl).

physiological conditions can reach 0.3 mM, HNE accumulates at concentrations up to 5 mM in cellular membranes under conditions of oxidative insults [5,6]. However, other RAs, such as 4-oxo-2E-nonenal (ONE) [7], 4-hydroxy-2E-hexenal (HHE) [8], and 4-hydroxy-dodeca-(2E,6Z)-dienal (HDDE) [9] can also be formed in lesser amounts, depending on the initial radical reaction conditions and accessibility of PUFAs. Under physiological conditions, RAs are effectively transferred from the cellular membrane into the cytosol, where they are metabolized by various enzymes, such as glutathione-S-transferases [10]. However, the reactive functional groups of RAs can also affect cellular molecules by (i) reacting with several amino acid residues in proteins [11], (ii) modifying the amine headgroups of membrane lipids [12] or (iii) targeting DNA [5,13]. The most common result of protein/lipid interaction with RAs is the formation of Michael adducts (MAs) and Schiff bases (SBs) [12,14]. Earlier, we proposed that the first mechanism of RA action (i) may be more relevant for the modification of cytosolic proteins, whereas the second mechanism (ii), which is much less understood, is important for the action of RAs on membrane transporters [12]. According to that mechanism, RA-PE adducts alter the biophysical properties of lipid bilayers, which in turn, alter the activity of membrane proteins [12], or may increase the permeability of the bilayer membrane, as shown for HNE [15].

In this study, we investigated the impact of HNE and ONE on the permeability of model membranes of various lipid compositions for protons and ions. For that purpose, we combined electrophysiological measurements of total membrane conductance (G_m) with molecular dynamics (MD) simulations. The quantum chemical (QM) calculations contributed to the understanding of the adduct structures used for MD simulations. Finally, we propose a novel mechanism of HNE action that is relevant for the membranes of cells with high lipid to protein ratio (such as oligodendrocytes) under conditions of oxidative stress.

2 Methods

2.1 Chemicals

DOPC, DOPE, CL, NaCl, Na_2SO_4, MES, TRIS, EGTA, hexane and hexadecane were purchased from Sigma Aldrich GmbH (Germany). 4-ONE and 4-HNE were purchased from Cayman Chemical (Ann Arbor, MI, USA) or synthesized as previously described [16]. *E. coli* polar lipids were purchased from Avanti@ Polar Lipids, Inc. (Alabaster, AL, USA).

2.2 Formation of planar bilayer membranes and measurements of electrical parameters

Planar lipid bilayers were formed from liposomes on the tips of plastic pipettes [17]. Membrane formation and bilayer quality were monitored by capacitance measurements. The capacitance was typically (0.73 ± 0.02) μF/cm^2 and did not depend on reactive aldehyde content. Current–voltage (I–V) characteristics were measured by a patch-clamp amplifier (EPC10, HEKA Elektronik, Dr. Schulze GmbH, Germany). Total membrane conductance was calculated from experimental data (I) obtained at applied voltages from - 50 mV to + 50 mV as previously described [17]. Liposomes were incubated with each RA for 15 min at 32 °C and pH 7.32.

2.3 Molecular dynamics simulations

Molecular dynamics (MD) simulations were performed for lipid bilayers of different compositions (Table 1) in aqueous solutions containing 0.1 M NaCl. Adducts were chosen based on the mass spectrometry (MS) results [12]. Chemical structures of the corresponding RA-DOPE adducts are shown in Fig. 3. 1,2-dioleoyl-sn-glycero-3-phosphocholine (DOPC), 1,2-dioleoyl-sn-glycero-3-phosphoethanolamine (DOPE), HNE-Michael adduct, HNE-Schiff adduct, ONE-Schiff adduct, HNE-double Michael adduct, and HNE-double Schiff adduct were described with Slipids force field [18–20]. Cardiolipin was not taken into account. When needed, all missing bonding and non-bonding parameters of RA-DOPE adduct molecules in the existing Slipids force field were updated with compatible CHARMM36 parameters [21]. Atomic charges were re-calculated by the standard Slipids procedure using the Merz-Singh-Kollman scheme [22], which consisted of B3LYP/6-31G(d) geometry optimization of the molecule of interest, a subsequent single point ESP charge calculation performed using the B3LYP/cc-pVTZ method and a final charge refinement performed using the RESP method [23].

Bilayers containing 128 lipid molecules were constructed by placing individual lipids on an 8 × 8 grid; this resulted in a bilayer of two monolayers each containing 64 individual lipid molecules. In the same way, adduct molecules were distributed in the leaflets instead of DOPE molecules. All systems were placed in a unit cell and solvated with ca. 12,000 water molecules by using the TIP3P water model [24]. In all simulations, 20 sodium ions were added to the system [25], which roughly corresponded to a NaCl concentration of 0.1 mol dm^{-3}. This Na^+ concentration was comparable to that used in the electrophysiological experiments. The size of the unit cell was approximately 6.5 × 6.5 × 12.0 nm. 3D periodic boundary conditions were employed along with long-range electrostatic interactions that were cut beyond the non-bonded cut-off of 1 nm by using the particle-mesh Ewald procedure [26] with a Fourier spacing of 1.2 nm. Real space Coulomb interactions were cut off at 1 nm, while van der Waals interactions were cut-off at 1.4 nm. We performed independent simulations with semi-isotropic pressure coupling in directions that were parallel and perpendicular to the bilayer normal using the Parrinello–Rahman algorithm [27]. The pressure was set to 1 bar and a coupling constant of 10 ps^{-1} was employed. All independent simulations for the lipid water sub-systems were performed at 310 K and controlled with a Nose–Hoover thermostat [28] with the coupling constant of 0.5 ps^{-1}. Bond lengths within the simulated molecules were constrained using the LINCS [29]. Water bond lengths were kept constant by using the SETTLE method [30]. Equations of motion were integrated using the leap-frog algorithm with a time step of 2 fs. Lipid bilayer membranes were initially equilibrated until a constant area per lipid was obtained (i. e. at least 10 ns for single adducts and up to 100 ns for double adducts), with a subsequent 100 ns simulation time used for analysis. Error bars for area per lipid were calculated as the difference between area per lipid for a full simulation time of 100 ns and the area per lipid as calculated for the final 50 ns of simulation.

The potential of mean forces (PMFs) for all systems were calculated using the setup where Na^+ ions were first inserted into the membrane at selected positions separated by at least 3 nm in the *z*-axis of the bilayer, thus ensuring that there were at least two Na^+ ions in the

bilayer at the same time. It was previously shown that a setup with multiple solutes inserted at the same time considerably reduced computational cost and statistical errors in the standard umbrella simulations, where a single solute was kept in the bilayer [31]. Water molecules that overlapped with Na^+ ions were removed. After proper minimization of the system, a harmonic umbrella potential of 1000 kJ mol^{-1} nm^{-2} was applied between Na^+ ions and the center of lipid mass. The distance between sodium ions was constantly monitored throughout the course of umbrella sampling simulations, which were used to calculate PMFs via the WHAM procedure [32]. The diffusion coefficient of Na^+ in the bilayer along the *z*-axis $D(z)$ was calculated from restrained simulations used in umbrella sampling simulations from the integral over the autocorrelation function of the z position of each sodium ion in the bilayer [33]. Because computation of diffusion coefficients from autocorrelation functions can be influenced by their long exponential decay, we integrated the autocorrelation function until it decayed to 0.01 × var (z), and thereby eliminated any noise around zero from the integration [34].

Error bars for free energies were estimated using the bootstrapping method, with 100 bootstraps on symmetrized free energy curves. Error bars for diffusion coefficients were estimated as the difference between symmetrized and unsymmetrized profiles along the *z*-axis. Permeability coefficients (P) were calculated from equation (1) assuming the standard inhomogeneous insolubility diffusion model [35,36]:

$$P = \int_{z_1}^{z_2} \frac{\exp\left(\frac{\Delta G(z)}{k_B T}\right)}{D(z)} dz \quad (1)$$

where z_1 and z_2 are located in the water phase, and $\Delta G(z)$ is the difference between the free energy at position z and the water phase (where it is assumed to be zero). MD simulations were performed using the GROMACS software package, version 4.6.3 [37].

2.4 Quantum chemical calculations

Quantum chemical calculations for the formation of RA-DOPE double adducts were performed in water (ε = 78.4) with one additional explicit water using the SMD solvation model [38] at 298 K and 1 bar. We used a simplified DOPE model in which the *sn*-1 and *sn*-2 acyl chains were removed and replaced with a methyl group, leaving the chemically important moiety intact. Also, the acyl chains have very large conformational flexibility and a considerable size which makes performing QM calculations unfeasible. All calculations were obtained using geometries optimized at the SMD/B3LYP/6-31G(d) level of theory [39,40], followed by MP2 single-point calculations at the SMD/MP2/6–311++G(d,p) level of theory [41,42]. Stationary points, minima and transition states on the potential energy surface were identified by vibrational analysis. Transition state structures were verified by the presence of one negative eigenvalue, and by inspecting the displacement along the vibrational mode corresponding to the single imaginary frequency. Gibbs free energies were calculated as the sum of single-point electronic energy and thermal correction to Gibbs free energy. Quantum chemical calculations were performed using Gaussian 09 software [43].

3 Results

3.1 Effect of ONE and HNE on bilayer membranes of various lipid compositions

To investigate the impact of RAs and RA-DOPE adducts on total membrane conductance (G_m), we formed planar lipid bilayer membranes from (*i*) DOPC:CL as a control; (*ii*) DOPE:DOPC:CL to mimic the inner mitochondrial membrane, and (*iii*) *E. coli* polar lipid extract (Fig. 1). We observed that in membranes composed of (ii) or (iii), G_m increased by more than 2-fold in the presence of HNE, but not in the presence of ONE. Neither HNE or ONE altered the G_m of DOPC:CL membranes. We assumed that the modification of DOPE by HNE led to the formation of various HNE-DOPE adducts [9,12], which might be responsible for the observed G_m increase. This assumption was supported by a HNE-concentration dependent increase in G_m (Fig. S5). In contrast, the formation of SB-ONE-DOPE adducts [12] and the presence of RAs in PE-free membranes did not alter G_m (Fig. 1).

Next, we estimated the Nernst potential [44,45] to determine the ion specificity of the G_m increase. For this purpose, we generated a pH gradient of 0.4 across the membrane using TRIS and kept the ionic strength and concentration of other ions constant. From I–V characteristics we obtained the reversal potential V_0 = 8 mV (Fig. 2, A). From the shift in V_0, we calculated that proton conductance ($G_{H+/OH-}$) accounted for only 1/3 of the G_m. It implies that increase in G_m in the presence of HNE-DOPE adducts was due to increase of sodium permeability. To support this result, we investigated the dependence of the observed increase in G_m on the sodium concentration. Fig. 2, B shows that increase in G_m correlated with the increased NaCl concentration in the range 50 mM – 150 mM at a constant pH if HNE was present. In contrast, G_m values were independent of ionic strength of buffer solution after the addition of 4-ONE (Fig. 2, B). Notably, 150 mM was the highest NaCl concentration at which the membranes were stable in the presence of HNE. In contrast, membranes remained stable up to a 500 mM NaCl concentration and G_m values remained unchanged when no RA was added. Our results suggest that the increase in G_m at different NaCl concentrations was due to the increase in Na^+ permeability mediated by DOPE-HNE adducts (Fig. 2, B). We excluded a partial contribution of anion Cl^- to the G_m increase because (i) anionic lipids such as CL, PG and RA-modified PEs strongly increased the negative surface potential of a lipid bilayer membrane [11], and (ii) a similar concentration of sodium in Na_2SO_4 buffer (Fig. 1) produced roughly the same effect on G_m. We obtained $P = (5.70 \pm 0.14) \times 10^{-11}$ cm s^{-1} from the linear increase in G_m (Fig. 2, B) by using the Goldman-Hodkin-Katz flux equation [46]. The permeability of Na^+ ($(0.5–2.9) \times 10^{-14}$ cm s^{-1} [47]) in intact phospholipid bilayers is several orders of magnitude lower than that of H^+ (~ $(0.3–1.8) \times 10^{-6}$ cm s^{-1} [48,49]), and therefore is independent of the Na^+ concentration in buffer (Fig. 2, B, grey bars).

3.2 Reaction mechanism for RA-PE double adduct formation

We modeled the effects of various Michael adducts and Schiff base adducts of DOPE on the biophysical properties of various bilayers (Table 1). We and other groups had previously reported the formation of single Michael and Schiff base adducts between HNE/ONE and DOPE, as determined by MS [12,50,51] and molecular dynamics simulations [51] (Fig. 3,

A). Therefore, we first investigated the reaction mechanism that leads to double Michael and Schiff adducts (numbered as **4** and **7**), which to date, have not been computationally predicted (Fig. 3, A). Mass spectrometry has been used to determine the structures of double adducts in the gas phase [12]. However, no mechanism leading to the formation of these products has been proposed. Based on the mechanism by which PE lipids react with dichloromethane and lysine in different mixtures of organic solvents and water [52], we suggested a possible mechanism leading to the formation of more relevant adducts of the same mass in the water phase (Fig. 3, B). Fig. S1 shows the energetics of the reaction and free energy barriers obtained by QM calculations. Our analysis of the energetic data showed that model double adducts **4** and **7** were readily formed in water (with free energy barriers up to 150 kJ mol^{-1}) and were thermodynamically stable when compared with initial reactants **1** and **5a**, respectively. Moreover, the suggested mechanism explains why no double Schiff adducts were formed when ONE was added – namely, the loss of water via protonation of the hydroxyl group in the steps **5a** to **6a** was not possible in the case of ONE. In particular, the loss of one water molecule occurred via protonation of hydroxyl group in HNE (Fig. 3). In contrast, ONE has a carbonyl group (Table 1), and its protonation cannot result in loss of a water molecule. Based on the quantum chemical data and reaction mechanism, we used the described full length double Michael and double Schiff adducts (Fig. 3) in our subsequent MD simulations.

3.3 MD simulations of RA-PE adducts position in a bilayer membrane

In order to understand how different RA-PE adducts alter the structure of lipid bilayers, we performed a series of MD simulations of bilayer lipid membranes in a 0.1 M NaCl solution (Table 1). We calculated the number density profiles of nitrogen, the oxygen atom of hydroxyl groups, the terminal carbon atoms of RA-PE-adducts, and the oxygen atom of water (Fig. 4), as well as nitrogen and phosphate atoms in the headgroups of DOPC, DOPE, RA-DOPE, and sodium ions (Fig. S4). As determined earlier by MS analysis and suggested by QM calculations (Fig. 3), HNE reacts with DOPE to form four types of adducts: a single Michael adduct (MA-HNE), a Schiff base adduct (SB-HNE), a double Michael adduct (D-MA-HNE), and a double Schiff adduct (D-SB-HNE). In contrast, 4-ONE and DOPE react to form only the SB-ONE adduct [12]. Because the ratios of the formed HNE-PE adducts are unknown, and to better visualize changes in the bilayer structure, we analyzed each individual adduct in a two component lipid bilayer membrane, DOPC:RA-PE.

In the intact DOPC:DOPE lipid bilayer, the nitrogen (N) and phosphorus (P) in DOPE were located at similar positions close to the P atom in DOPC, (Figs. S4 and A). In each of the RA-adducts the distributions of N atom positions (Fig. 4, A-E; Table S1) were moved to the bilayer center as compared to N(DOPE) (Fig. 4, A). The corresponding oxygen atoms of hydroxyl groups, O(MA), and O(SB) of HNE-PE adducts were slightly shifted to the hydrophobic interior (Fig. 4A–E). The terminal carbon atoms of the hydrocarbon tail in the HNE-PE adducts - C(MA) and C(SB) - were markedly pushed into the hydrophobic core, with the number density maximum located in the hydrophobic region (Fig. 4A–E) at ca. 1 nm from the bilayer center. The number density profiles of selected SB-HNE atoms (Fig. 4, C) were very similar to those of MA-HNE adducts (Fig. 4, B). This is because an identical hydrogen bonding opportunity exists for both HNE adducts when the –OH group is present

in both adducts and can readily form a hydrogen bond with the DOPC phosphate group. In contrast, O(SB) and C(SB) atoms of the SB-ONE adducts were located in the headgroup region (Fig. 4, F) due to the inability of the keto-group to form a favorable hydrogen bond with the DOPC phosphate group, as shown in previous studies [12]. The distributions of the selected atoms of the D-MA-HNE adduct (Fig. 4, D) were very similar to those of single HNE adducts (Fig. 4B and C), with one additional hydrocarbon chain being inserted into the bilayer, resulting a large increase in the calculated area per lipid. Finally, when the different distributions of the selected groups of D-SB-HNE-adducts were compared with the distributions of the RA-PE adducts, the D-SB-HNE-adducts showed a non-negligible localization of adduct terminal carbon atoms, C(SB) in the bilayer center, and a shift of O(SB) atoms toward the hydrophobic core (Fig. 4, E). The difference in the distribution of C(SB) was due to the fact that hydrophobic tails of D-SB-HNE adducts do not have hydrogen bond donors, and therefore insert deeper into the hydrophobic core as a result of hydrophobic interactions with acyl chains.

A comparison of the structural properties of lipid bilayers in terms of area per lipid and hydrophobic core thickness revealed RA-PE-specific alterations (Fig. 5A and B). We found that the calculated areas per lipid were similar for systems with MA-HNE and SB-HNE adducts, when assuming values of A = 0.728 nm^2 and A = 0.724 nm^2 (Fig. 5, A), whereas the smallest increase in area per lipid was found for the SB-ONE-adduct (A = 0.704 nm^2). On the other hand, the calculated area per lipid for systems with double adducts increased significantly. The area per lipid value (A) was 0.808 nm^2 for D-MA-HNE-adducts and increased to 0.852 nm^2 for D-SB-HNE-adducts, which was a 30% increase when compared to the neat bilayer. A comparison of bilayer hydrophobic thickness using the number density of water at 1 nm^{-3} revealed thinning of the bilayers in the presence of RA-PEs. This thinning was particularly evident in the lipid bilayer with D-SB-HNE adducts, in which thickness decreased by 20% when compared with the neat bilayer (Fig. 5, B). Thinning of the hydrophobic core, and especially in the presence of double adducts (D-MA-HNE and D-SB-HNE), indicated a significant expansion of the lipid bilayers, which was in agreement with the calculated areas per lipid (Fig. 5, A). The overall increase that occurs in area per lipid upon substitution of a DOPE lipid with RA-PE depends on (i) the structure of the RA-PE-adducts (Fig. 3) and (ii) the position of the additional hydrocarbon tail(s) in the lipid bilayer, as shown in the number density profiles (Fig. 4).

In summary, our results from direct MD simulations indicate in the case of double adducts (D-MA-HNE and D-SB-HNE) that the bilayers were significantly expanded and thinned. These are the main structural factors that influence ion permeability, as suggested by the free energy calculations presented below.

3.4 Changes in free energy barrier, diffusion coefficients, and membrane permeability due to the HNE-mediated modification of DOPE

MD simulations revealed qualitative differences in the free energy barrier (ΔG, Fig. 6, A) and permeability (P, Fig. 6, B) of Na^+ when passing through bilayer membranes containing various RA-PE adducts. The ΔG for translocation of Na^+ was highest in the DOPC:DOPE lipid bilayer (ΔG = 82.5 kJ mol^{-1}), and was slightly lower in lipid bilayers containing SB-

HNE and SB-ONE adducts. The decrease in ΔG was more pronounced in lipid bilayers with single and double MA-HNE adducts, where ΔG decreased by approx. 14% and 23%, respectively. The largest decrease in ΔG (~30%, assuming a value of 59 kJ mol^{-1}) occurred when using lipid bilayers containing D-SB-HNE adducts (Fig. 6, A). Next, we used the standard inhomogeneous insolubility diffusion model to calculate P_{Na} in those systems [35,53]. For the neat lipid bilayer, we obtained $P_{Na} = 5.5 \times 10^{-13}$ cm s^{-1}, which was very close to the experimental value ($P \sim 10^{-14}$ cm s^{-1}) [47,54], and thus validated the chosen computational method (Fig. 6 B). Consistent with the change in ΔG, the smallest increase in P_{Na} was obtained for SB-HNE and SB-ONE adducts (Table S2). Introduction of MA-HNE adducts increased P_{Na} by two orders of magnitude ($P = 2.8\times 10^{-11}$ cm s^{-1}), while the presence of double adducts (D-MA-HNE and D-SB-HNE) in a lipid bilayer membrane resulted in a stronger P_{Na} increase (three and four orders of magnitude, respectively; Fig. 6, B; Table S2). The results of our MD simulations suggest that a combination of MA-HNE adducts with D-MA-HNE and D-SB-HNE adducts in a lipid bilayer membrane can increase the membrane's permeability, which fits with the estimated permeability value obtained from our electrophysiological studies ($P = 5.7 \times 10^{-11}$ cm s^{-1}). A decrease in the ΔG for ion translocation and an increase in P are reflected in structural changes in the lipid bilayers, such as their increased calculated area per lipid and bilayer thinning (Fig. 5, A-B).

4 Discussion

Electrophysiological experiments showed that the G_m of a neat lipid bilayer membrane was increased in the presence of HNE but not ONE. We and other groups previously reported that HNE and ONE form different membrane-active adducts with the amino group of PE, such as MA-HNE, SB-HNE, and SB-ONE [12,55]. Although double adducts of HNE were also recorded, no effect on the activity of the proton and ion transporters (UCPs, valinomycin, and CCCP) could be attributed to their action [12]. The effect of ONE on proton transport was suggested to result from formation of SB-ONE, because no other adducts were found. The anchoring of a SB-ONE adduct in the lipid headgroup region was responsible for changes in the membrane order parameter and boundary potential. Furthermore, we suggested membrane curvature alteration, generated by formation of PE-adducts, as another important factor that modulates UCP1 activity [56]. Our present study demonstrated that SB-ONE adducts (in contrast to double HNE adducts) do not influence membrane ion permeability in protein-free membranes.

Our calculation of the Nernst potential in the presence of a proton gradient revealed that the HNE-mediated increase in G_m in neat lipid membranes was mainly caused by sodium ions rather than by protons. Molecular dynamics simulations suggested that the increase in Na^+ permeability by four orders of magnitude (from $P = 5.5\times 10^{-13}$ to $P = 4.8 \times 10^{-9}$ cm s^{-1}) occurred when using a bilayer composed of DOPC and D-SB-HNE adducts. Significant contributions to that increase were also made by single and double MA ($P = 2.8 \times 10^{-11}$ to $P = 4.0 \times 10^{-10}$ cm s^{-1}), while the calculated membrane permeabilities due to SB adducts were below the permeability estimated by our electrophysiological measurements ($P = 5.7 \times 10^{-11}$ cm s^{-1}). While hydrophobic tails of double adducts insert deeper in the hydrophobic core of a lipid bilayer membrane (Fig. 3, B and 4, F), that deep insertion results in an increased area per lipid (Fig. 5, A) and a decrease in ΔG (Fig. 6, A). The larger area per lipid

alters the water profile across the lipid bilayer, making it thinner (Fig. 5, B) and more permeable to Na^+ ions (Fig. 6, B and Fig. 7). This was not the case for the membranes without PE (Fig. 1). Phosphatidylserine and sphingomyelin may help to increase membrane permeability via a similar mechanism, because of a possible interaction between HNE and amino groups. However, further investigations are needed to support that hypothesis.

Active ion translocation in cells is maintained by sophisticated cellular machinery that includes a variety of ion channels [57,58]. The physiological equilibrium of ions across a cell membrane is especially important for the ability of cells such as neurons, cardiomyocytes, and neurosensory cells to generate action potentials. RAs, which are produced under conditions of oxidative stress, are known to affect both cellular membranes and proteins. Here, we showed for the first time that formation of RA-PE adducts influences the ion permeability of neat lipid bilayer membranes.

There is no kinetic data about reaction rate of HNE with the amino group of PE. Rate constants were studied for the reaction of HNE with amino acids/peptides [59]. The reactivity of amino acids toward HNE was: cysteine > > histidine > lysine, indicating that reactivity of thiol group-containing cysteines is higher than amino group-containing lysines and histidines. It may imply that HNE would primary attack thiol groups of proteins. It's why the interaction with the amino group of PE may be more relevant for membranes with low protein/lipid ratio (e.g. oligodendrocytes). The increased ion permeability of membranes may contribute to enhanced spontaneous electrical activity of pacemaker cells in the heart, leading to abnormalities such as arrhythmia, impaired pumping capability, and reduced cardiac output. Furthermore, the additional sodium leak in brain cells may result in neuronal hyper-excitability [60]. The involvement of ROS in neurodegenerative diseases and aging can be partially explained by the here-described lipid-mediated mechanism. The effects of RAs on lipid bilayer membranes, which depend on the membrane's PE content, can be applied to develop new compounds that alter the characteristics of cells that contain increased levels of PE, such as cancer cells. Ophiobolin, which is known for its selective antitumor activity and cytotoxicity [61], was reported to bind to PE and destabilize a membrane. It might be expected that highly specialized cells with low protein to lipid ratios and high PE abundance in their plasma membranes, such as oligodendrocytes (0.25) [62], are affected by RAs, mainly by the mechanism described here. Although the mean RA concentrations that have been measured in cells are lower than those used in the present study, the local RA concentration in the membrane can reach millimolar concentrations under oxidative stress [5].

In summary, we showed that the increase in the total membrane conductance of neat PE-containing bilayers upon addition of HNE was mainly due to an increase in the membrane's permeability to cations in the buffer solution (Fig. 7). MD simulations, supported by quantum chemical calculations related to the mechanism for HNE double adduct formation, revealed the increase of sodium ion permeability by three to four order of magnitude only for the system that contained D-MA-HNE and D-SB-HNE. These increases were due to decreases in membrane thickness and bilayer thinning produced by those particular types of adducts. In contrast, while modification of PE by ONE led to the greatest change in transmembrane protein function, it did not affect conductance of the neat lipid bilayer. Taken

Europe PMC Funders Author Manuscripts

together, our results demonstrate the ability of RAs to affect the function of cells via several different mechanisms.

Supplementary Material

Refer to Web version on PubMed Central for supplementary material.

Acknowledgments

This work was supported by the Croatian Science Foundation (project no. UIP-2014-09-6090 to M.V.) and the Austrian Research Fund (FWF, P25123 to E.P.). The computational part of the research was performed using the resources of the computer cluster Isabella, based in the SRCE-University of Zagreb University Computing Center. We also thank Dr. Katarina Vazdar for synthesizing 4-HNE and 4-ONE and Dr. Peter Pohl for his helpful comments during preparation of the manuscript.

Abbreviations

RA	reactive aldehydes
4-ONE	4-oxo-2-nonenal
4-HNE	4-hydroxy-2- nonenal
DOPE	1,2-Dioleoyl-sn-glycero-3-phosphoethanolamine
DOPC	1,2-dioleoyl-sn-glycero-3-phosphocholine
CL	cardiolipin

References

[1]. Murphy MP. How mitochondria produce reactive oxygen species. Biochem J. 2009; 417(1):1–13. [PubMed: 19061483]

[2]. Fruhwirth GO, Loidl A, Hermetter A. Oxidized phospholipids: from molecular properties to disease. Biochim Biophys Acta. 2007; 1772(7):718–736. [PubMed: 17570293]

[3]. Catala A. Lipid peroxidation of membrane phospholipids generates hydroxy-alkenals and oxidized phospholipids active in physiological and/or pathological conditions. Chem Phys Lipids. 2009; 157(1):1–11. [PubMed: 18977338]

[4]. Yin H, Xu L, Porter NA. Free radical lipid peroxidation: mechanisms and analysis. Chem Rev. 2011; 111(10):5944–5972. [PubMed: 21861450]

[5]. Esterbauer H, Schaur RJ, Zollner H. Chemistry and biochemistry of 4-hydroxynonenal, malonaldehyde and related aldehydes. Free Radic Biol Med. 1991; 11(1):81–128. [PubMed: 1937131]

[6]. Uchida K. 4-Hydroxy-2-nonenal: a product and mediator of oxidative stress. Prog Lipid Res. 2003; 42(4):318–343. [PubMed: 12689622]

[7]. Lee SH, Oe T, Blair IA. Vitamin C-induced decomposition of lipid hydroperoxides to endogenous genotoxins. Science. 2001; 292(5524):2083–2086. [PubMed: 11408659]

[8]. Van Kuijk FJ, Holte LL, Dratz EA. 4-Hydroxyhexenal: a lipid peroxidation product derived from oxidized docosahexaenoic acid. Biochim Biophys Acta. 1990; 1043(1):116–118. [PubMed: 2138035]

[9]. Bacot S, Bernoud-Hubac N, Baddas N, Chantegrel B, Deshayes C, Doutheau A, Lagarde M, Guichardant M. Covalent binding of hydroxy-alkenals 4-HDDE, 4-HHE, and 4-HNE to ethanolamine phospholipid subclasses. J Lipid Res. 2003; 44(5):917–926. [PubMed: 12588949]

[10]. Alary J, Gueraud F, Cravedi JP. Fate of 4-hydroxynonenal in vivo: disposition and metabolic pathways. Mol Asp Med. 2003; 24(4–5):177–187.

[11]. Zarkovic N, Cipak A, Jaganjac M, Borovic S, Zarkovic K. Pathophysiological relevance of aldehydic protein modifications. J Proteomics. 2013; 92:239–247. [PubMed: 23438936]

[12]. Jovanovic O, Pashkovskaya AA, Annibal A, Vazdar M, Burchardt N, Sansone A, Gille L, Fedorova M, Ferreri C, Pohl EE. The molecular mechanism behind reactive aldehyde action on transmembrane translocations of proton and potassium ions. Free Radic Biol Med. 2015; 89:1067–1076. [PubMed: 26520807]

[13]. Galligan JJ, Rose KL, Beavers WN, Hill S, Tallman KA, Tansey WP, Marnett LJ. Stable histone adduction by 4-Oxo-2-nonenal: a potential link between oxidative stress and epigenetics. J Am Chem Soc. 2014; 136(34):11864–11866. [PubMed: 25099620]

[14]. Schaur RJ. Basic aspects of the biochemical reactivity of 4-hydroxynonenal. Mol Asp Med. 2003; 24(4–5):149–159.

[15]. Malingriaux EA, Rupprecht A, Gille L, Jovanovic O, Jezek P, Jaburek M, Pohl EE. Fatty acids are key in 4-hydroxy-2-nonenal-mediated activation of uncoupling proteins 1 and 2. PLoS One. 2013; 8(10):e77786. [PubMed: 24204965]

[16]. Zimmermann L, Moldzio R, Vazdar K, Krewenka C, Pohl EE. Nutrient deprivation in neuroblastoma cells alters 4-hydroxynonenal-induced stress response. Oncotarget. 2017; 8(5):8173–8188. [PubMed: 28030790]

[17]. Beck V, Jaburek M, Breen EP, Porter RK, Jezek P, Pohl EE. A new automated technique for the reconstitution of hydrophobic proteins into planar bilayer membranes. Studies of human recombinant uncoupling protein 1. Biochim Biophys Acta. 2006; 1757(5–6):474–479. [PubMed: 16626624]

[18]. Jaembeck JP, Lyubartsev AP. An extension and further validation of an all-atomistic force field for biological membranes. J Chem Theory Comput. 2012; 8(8):2938–2948. [PubMed: 26592132]

[19]. Jaembeck JP, Lyubartsev AP. Derivation and systematic validation of a refined all-atom force field for phosphatidylcholine lipids. J Phys Chem B. 2012; 116(10):3164–3179. [PubMed: 22352995]

[20]. Jaembeck JPM, Lyubartsev AP. Another piece of the membrane puzzle: extending slipids further. J Chem Theory Comput. 2012; 9(1):774–784. [PubMed: 26589070]

[21]. Klauda JB, Venable RM, Freites JA, O'Connor JW, Tobias DJ, Mondragon-Ramirez C, Vorobyov I, MacKerell AD Jr, Pastor RW. Update of the CHARMM all-atom additive force field for lipids: validation on six lipid types. J Phys Chem B. 2010; 114(23):7830–7843. [PubMed: 20496934]

[22]. Singh UC, Kollman PA. An approach to computing electrostatic charges for molecules. J Comput Chem. 1984; 5(2):129–145.

[23]. Bayly CI, Cieplak P, Cornell WD, Kollman PA. A well-behaved electrostatic potential based method using charge restraints for deriving atomic charges - the resp model. J Phys Chem. 1993; 97(40):10269–10280.

[24]. Jorgensen WL, Chandrasekhar J, Madura JD, Impey RW, Klein ML. Comparison of simple potential functions for simulating liquid water. J Chem Phys. 1983; 79(2):926–935.

[25]. Åqvist J. Ion-water interaction potentials derived from free energy perturbation simulations. J Phys Chem. 1990; 94(21):8021–8024.

[26]. Essmann U, Perera L, Berkowitz ML, Darden T, Lee H, Pedersen LG. A smooth particle mesh Ewald method. J Chem Phys. 1995; 103(19):8577–8593.

[27]. Parrinello M, Rahman A. Polymorphic transitions in single crystals: a new molecular dynamics method. J Appl Phys. 1981; 52(12):7182–7190.

[28]. Nosé S. A molecular dynamics method for simulations in the canonical ensemble. Mol Phys. 1984; 52(2):255–268.

[29]. Hess B, Bekker H, Berendsen HJ, Fraaije JG. LINCS: a linear constraint solver for molecular simulations. J Comput Chem. 1997; 18(12):1463–1472.

[30]. Miyamoto S, Kollman PA. SETTLE: an analytical version of the SHAKE and RATTLE algorithm for rigid water models. J Comput Chem. 1992; 13(8):952–962.

[31]. Zocher F, van der Spoel D, Pohl P, Hub JS. Local partition coefficients govern solute permeability of cholesterol-containing membranes. Biophys J. 2013; 105(12):2760–2770. [PubMed: 24359748]

[32]. Hub JS, de Groot BL, van der Spoel D. g_wham—a free weighted histogram analysis implementation including robust error and autocorrelation estimates. J Chem Theory Comput. 2010; 6(12):3713–3720.

[33]. Hummer G. Position-dependent diffusion coefficients and free energies from Bayesian analysis of equilibrium and replica molecular dynamics simulations. New J Phys. 2005; 7:34–34.

[34]. Dickson CJ, Hornak V, Pearlstein RA, Duca JS. Structure-kinetic relationships of passive membrane permeation from multiscale modeling. J Am Chem Soc. 2017; 139(1):442–452. [PubMed: 27951634]

[35]. Diamond JM, Katz Y. Interpretation of nonelectrolyte partition coefficients between dimyristoyl lecithin and water. J Membr Biol. 1974; 17(2):121–154. [PubMed: 4407798]

[36]. Shinoda W. Permeability across lipid membranes. Biochim Biophys Acta Biomembr. 2016; 1858(10):2254–2265.

[37]. Hess B, Kutzner C, Van Der Spoel D, Lindahl E. GROMACS 4: algorithms for highly efficient, load-balanced, and scalable molecular simulation. J Chem Theory Comput. 2008; 4(3):435–447. [PubMed: 26620784]

[38]. Marenich AV, Cramer CJ, Truhlar DG. Universal solvation model based on solute electron density and on a continuum model of the solvent defined by the bulk dielectric constant and atomic surface tensions. J Phys Chem B. 2009; 113(18):6378–6396. [PubMed: 19366259]

[39]. Becke AD. Density-functional thermochemistry. III. The role of exact exchange. J Chem Phys. 1993; 98(7):5648–5652.

[40]. Stephens PJ, Devlin FJ, Chabalowski CF, Frisch MJ. Ab initio calculation of vibrational absorption and circular dichroism spectra using density functional force fields. J Phys Chem. 1994; 98(45):11623–11627.

[41]. Hehre WJ, Ditchfield R, Pople JA. Self—consistent molecular orbital methods. XII. Further extensions of Gaussian—type basis sets for use in molecular orbital studies of organic molecules. J Chem Phys. 1972; 56(5):2257–2261.

[42]. Hariharan PC, Pople JA. The influence of polarization functions on molecular orbital hydrogenation energies. Theor Chim Acta. 1973; 28(3):213–222.

[43]. Frisch, MJ, Trucks, GW, Schlegel, HB, Scuseria, GE, Robb, MA, Cheeseman, JR, Scalmani, G, Barone, V, Mennucci, B, Petersson, GA. Gaussian 09, Revision A. 1. Gaussian Inc; Wallingford, CT: 2009.

[44]. Kreiter J, Pohl EE. A micro-agar salt bridge electrode for analyzing the poton turnover rate of recombinant membrane proteins. J Vis Exp. 2019; 143:e58552.

[45]. Urbankova E, Voltchenko A, Pohl P, Jezek P, Pohl EE. Transport kinetics of uncoupling proteins. Analysis of UCP1 reconstituted in planar lipid bilayers. J Biol Chem. 2003; 278(35):32497–32500. [PubMed: 12826670]

[46]. Ebert A, Hannesschlaeger C, Goss KU, Pohl P. Passive permeability of planar lipid bilayers to organic anions. Biophys J. 2018; 115(10):1931–1941. [PubMed: 30360927]

[47]. Hauser H, Oldani D, Phillips MC. Mechanism of ion escape from phosphatidylcholine and phosphatidylserine single bilayer vesicles. Biochemistry. 1973; 12(22):4507–4517.

[48]. Gutknecht J. Proton conductance through phospholipid bilayers: water wires or weak acids? J Bioenerg Biomembr. 1987; 19(5):427–442. [PubMed: 2826410]

[49]. Paula S, Volkov AG, van Hoek AN, Haines TH, Deamer DW. Permeation of protons, potassium ions, and small polar molecules through phospholipid bilayers as a function of membrane thickness. Biophys J. 1996; 70(1):339–348. [PubMed: 8770210]

[50]. Guichardant M, Taibi-Tronche P, Fay LB, Lagarde M. Covalent modifications of aminophospholipids by 4-hydroxynonenal. Free Radic Biol Med. 1998; 25(9):1049–1056. [PubMed: 9870558]

[51]. Vazdar K, Vojta D, Margetić D, Vazdar M. Reaction mechanism of covalent modification of phosphatidylethanolamine lipids by reactive aldehydes 4-Hydroxy-2-nonenal and 4-Oxo-2-nonenal. Chem Res Toxicol. 2017; 30(3):840–850. [PubMed: 28222263]

[52]. Škulj S, Vazdar K, Margetić D, Vazdar M. Revisited mechanism of reaction between model lysine amino acid side chain and 4-hydroxynonenal in different solvent environments. J Org Chem. 2019; 84(2):526–535. [PubMed: 30543108]

[53]. Marrink S-J, Berendsen HJC. Simulation of water transport through a lipid membrane. J Phys Chem. 1994; 98(15):4155–4168.

[54]. Palacios LE, Wang T. Egg-yolk lipid fractionation and lecithin characterization. J Am Oil Chem Soc. 2005; 82(8):571–578.

[55]. Guichardant M, Bernoud-Hubac N, Chantegrel B, Deshayes C, Lagarde M. Aldehydes from n-6 fatty acid peroxidation. Effects on aminophospholipids, Prostaglandins Leukot. Essent Fatty Acids. 2002; 67(2–3):147–149.

[56]. Chekashkina K, Jovanovic O, Kuzmin P, Pohl E, Pavel B. The changes of physical parameters of lipid membrane caused by lipid peroxidation-derived aldehydes. Biophys J. 2017; 112(3):520a.

[57]. Ahern CA, Payandeh J, Bosmans F, Chanda B. The hitchhiker's guide to the voltage-gated sodium channel galaxy. J Gen Physiol. 2016; 147(1):1–24. [PubMed: 26712848]

[58]. Dib-Hajj SD, Yang Y, Black JA, Waxman SG. The Na(V)1.7 sodium channel: from molecule to man. Nat Rev Neurosci. 2013; 14(1):49–62. [PubMed: 23232607]

[59]. Doorn JA, Petersen DR. Covalent modification of amino acid nucleophiles by the lipid peroxidation products 4-hydroxy-2-nonenal and 4-oxo-2-nonenal. Chem Res Toxicol. 2002; 15(11):1445–1450. [PubMed: 12437335]

[60]. Morris CE. Cytotoxic swelling of sick excitable cells - impaired ion homeostasis and membrane tension homeostasis in muscle and neuron. Curr Top Membr. 2018; 81:457–496. [PubMed: 30243439]

[61]. Chidley C, Trauger SA, Birsoy K, O'Shea EK. The anticancer natural product ophiobolin A induces cytotoxicity by covalent modification of phosphatidylethanolamine. Elife. 2016; 5:e14601. [PubMed: 27403889]

[62]. O'Brien JS, Sampson EL. Lipid composition of the normal human brain: gray matter, white matter, and myelin. J Lipid Res. 1965; 6(4):537–544. [PubMed: 5865382]

Europe PMC Funders Author Manuscripts

Europe PMC Funders Author Manuscripts

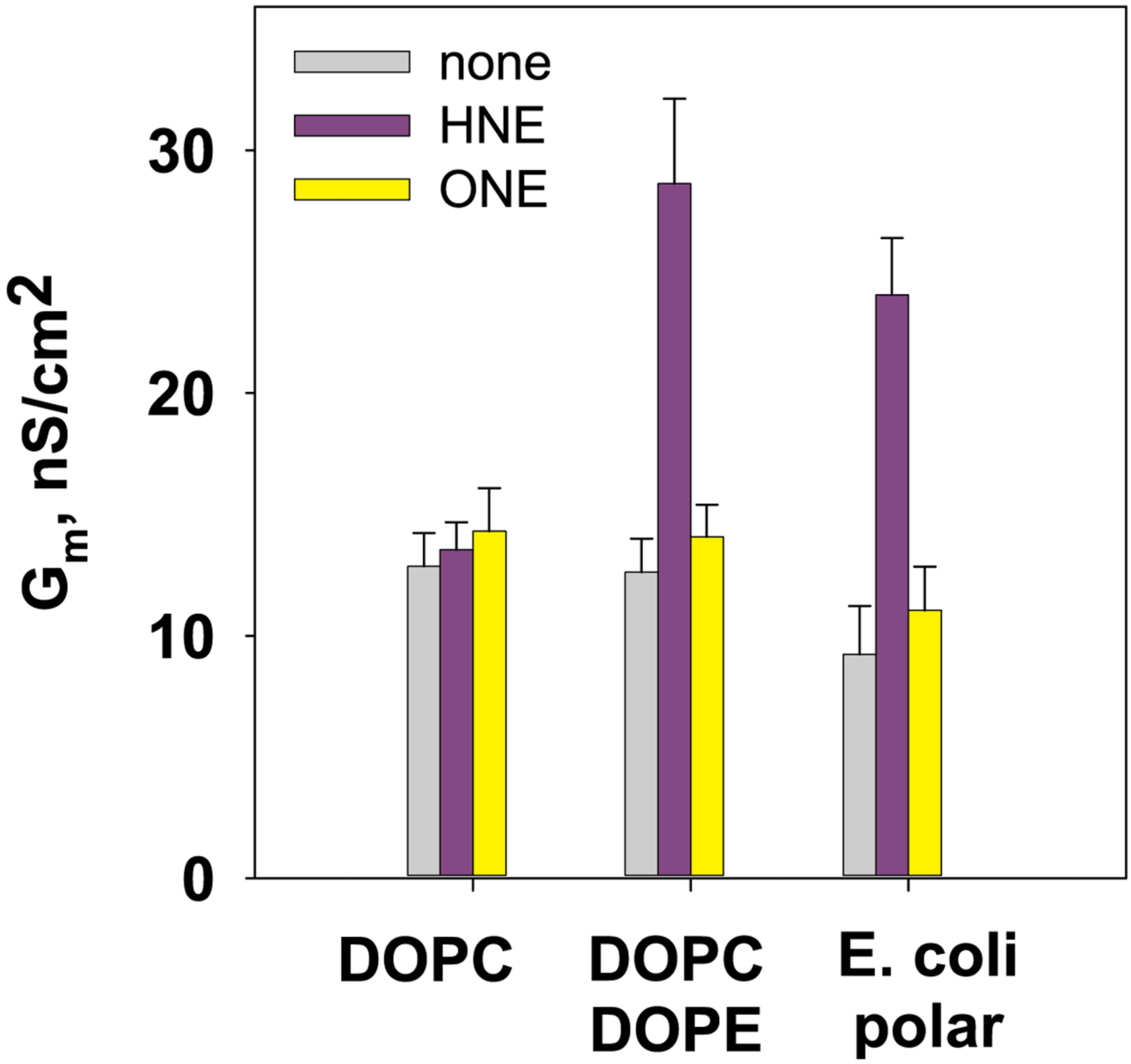

Fig. 1.

Effect of reactive aldehydes (HNE and ONE) on total membrane conductance (Gm). The lipid compositions of bilayer membranes were: DOPC:CL (90:10 mol%), DOPE:DOPC:CL (45:45:10 mol%), and *E. coli* polar lipid (PE:PG:CL, 71.4:23.4:5.2 mol%). The buffer solution contained 50 mM Na_2SO_4, 10 mM MES, and 10 mM TRIS at 32 °C and pH = 7.32. The concentrations of lipids and RAs were 1.2 mg/ml and 0.84 mM, respectively.

Europe PMC Funders Author Manuscripts

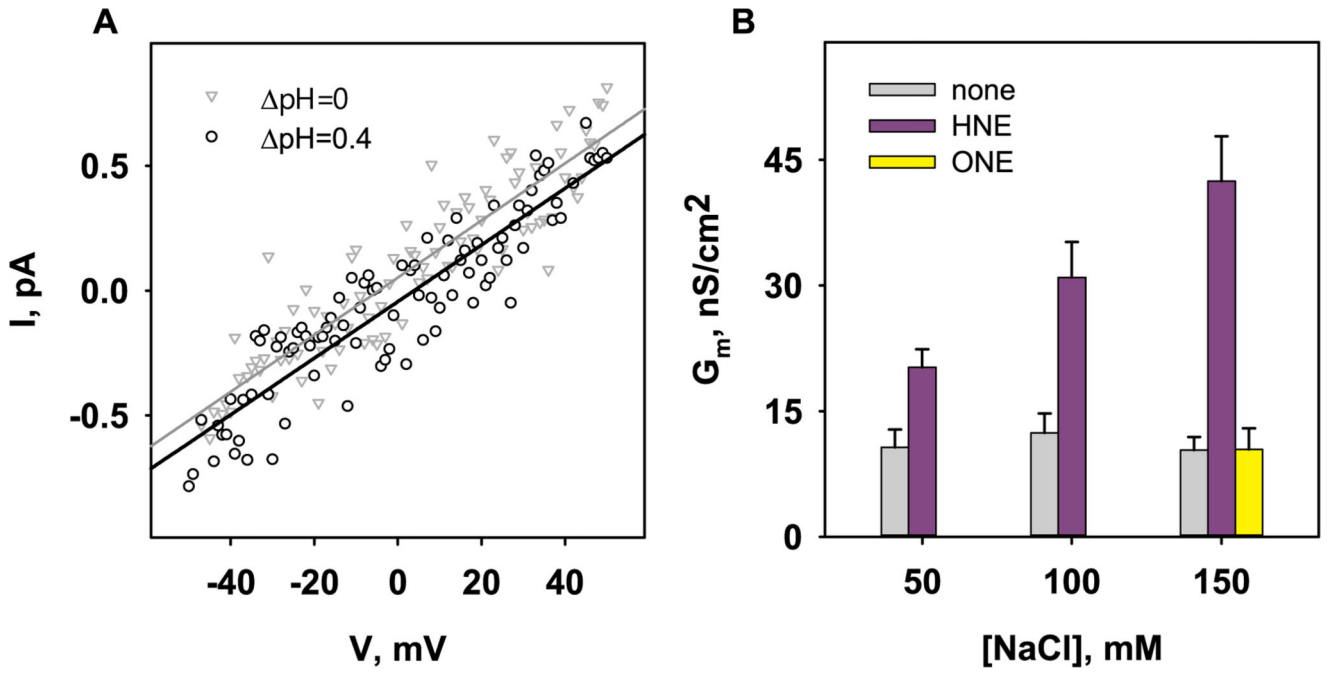

Fig. 2.

Influence of HNE-DOPE adducts on Na^+ and H^+ translocation. A. Representative current-voltage measurements in the presence (grey triangles) and absence (white dots) of a pH gradient of 0.4. The voltage shift is the difference in the x-axis intersection values of both measurements. The membranes were composed of DOPE:DOPC:CL (45:45:10 mol%). The buffer solution contained 50 mM Na_2SO_4, 10 mM MES, 10 mM TRIS, and 0.6 mM EGTA at 32°C and pH=7.32. B. Influence of the ionic strength of the buffer solution on total membrane conductance (Gm) in the presence of HNE or ONE. The membrane were composed of DOPE:DOPC (50:50 mol%). Besides NaCl, the buffer solution also contained 10 mM MES and 10 mM TRIS at 32°C and pH 7.32. The concentrations of lipids and RAs were 1.2 mg/ml and 0.84 mM, respectively.

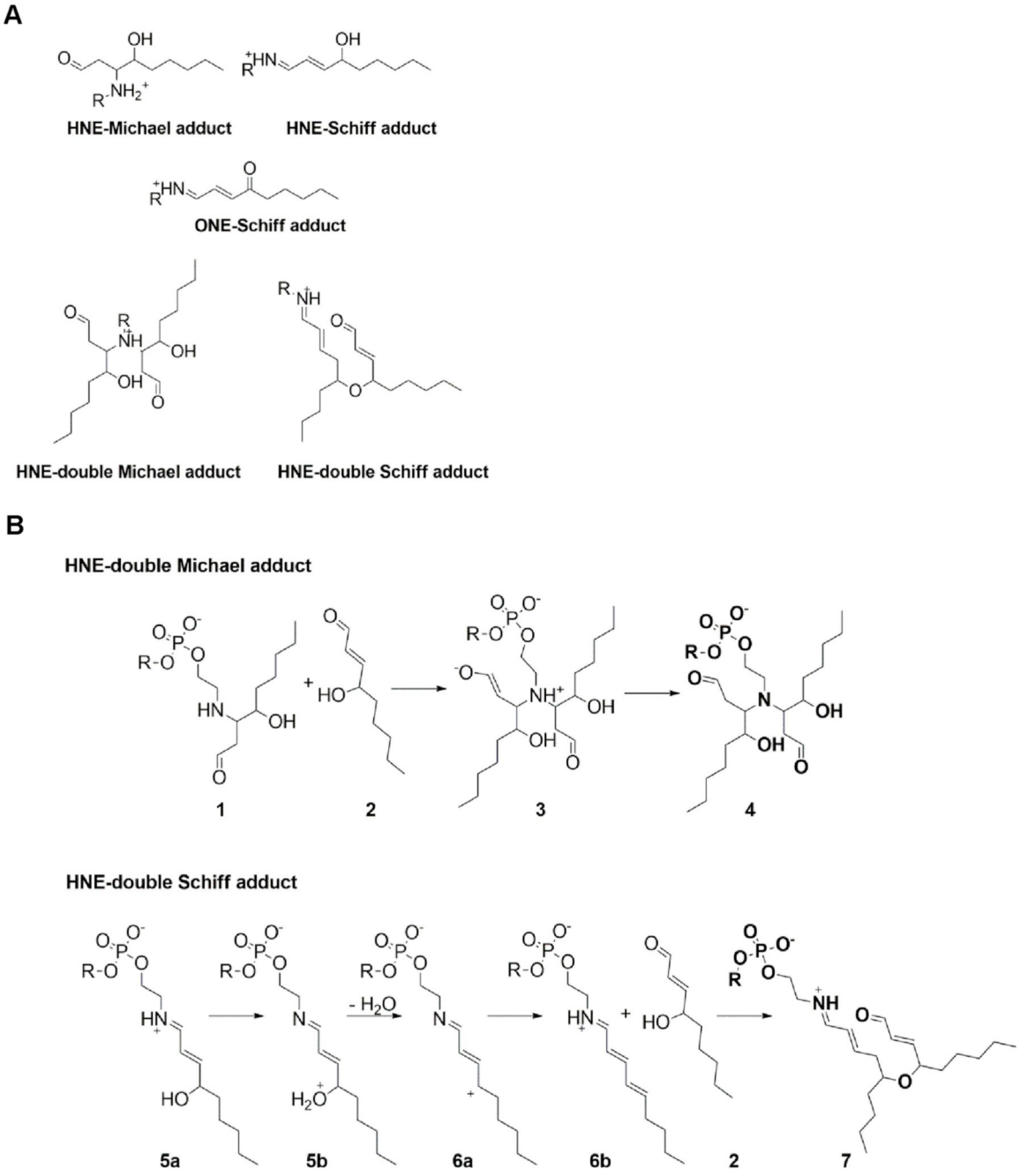

Fig. 3.

A. Chemical structures of DOPE adducts of HNE and ONE. B. Proposed reaction mechanism for HNE-double Michael adduct and HNE-double Schiff adduct formation. R stands for the rest of the DOPE lipid molecule.

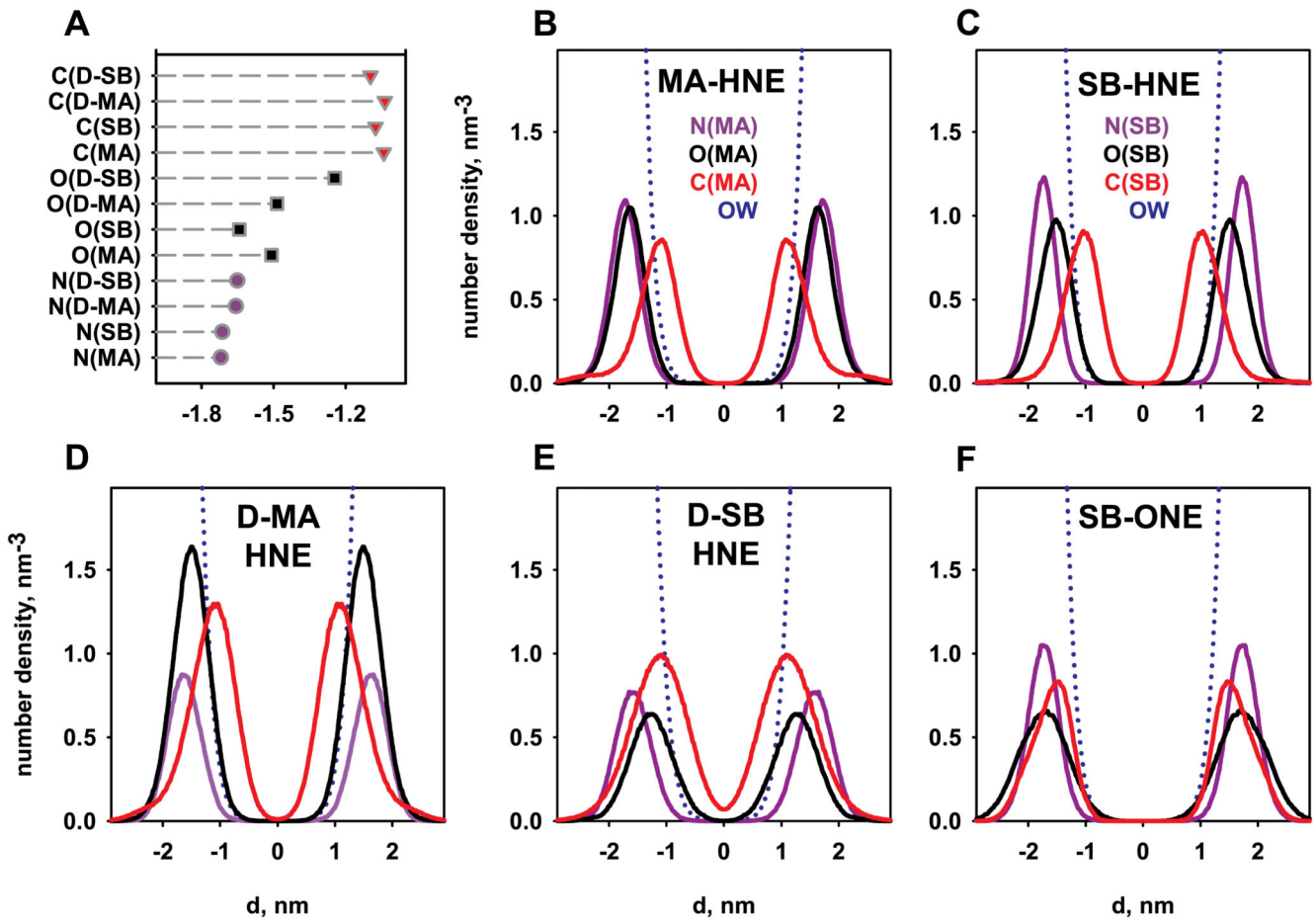

Fig. 4.

Average *z*-positions of the different groups calculated for HNE adducts (A), and the number density profiles for lipid bilayer membranes of different compositions (DOPC:MA-HNE (B), DOPC:SB-HNE (C), DOPC:D-MA-HNE (D), DOPC:D-SB-HNE (E), and DOPC:SB-ONE (F)). N(PE) stands for the nitrogen atom in the DOPE ammonium group. N(MA), O(MA) and C(MA) are nitrogen and oxygen in hydroxyl group, and terminal carbon atom of MA-HNE and D-MA-HNE, respectively. N(SB), O(SB) and C(SB) are nitrogen and oxygen in the hydroxyl group and terminal carbon atom of SB-HNE, D-SB-HNE, and ONE-Schiff base adducts, respectively. OW is the water oxygen atom.

Europe PMC Funders Author Manuscripts

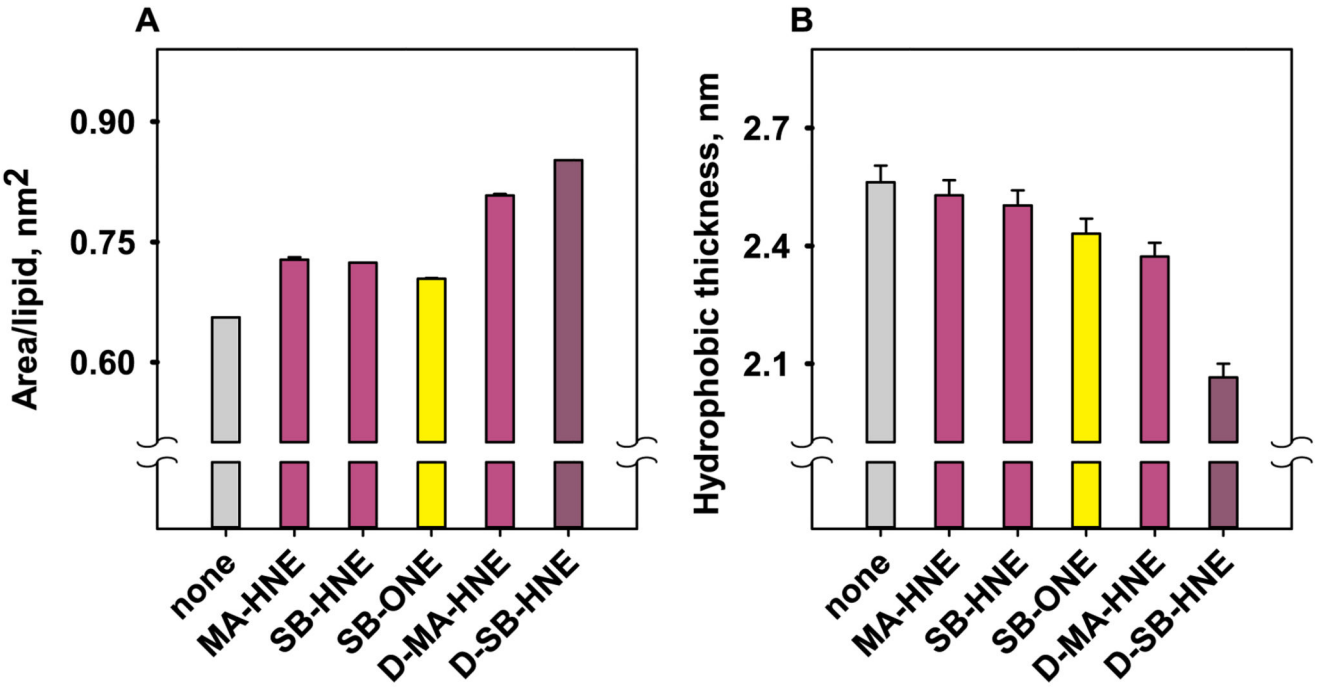

Fig. 5.

Influence of HNE and ONE adducts on area per lipid (A) and hydrophobic thickness (B) in membranes of different lipid compositions. Membranes were composed of DOPC:DOPE or DOPC:RADOPE (50:50 mol%). The RAs used were: the Michael adduct of HNE (MA-HNE), Schiff base adduct of HNE (SB-HNE), and Schiff base adduct of ONE (SB-ONE). D-MA-HNE and D-SB-HNE are double Michael adducts or Schiff base adducts of HNE. Hydrophobic thickness was calculated for OW ndp = 1 nm^{-3}.

Europe PMC Funders Author Manuscripts

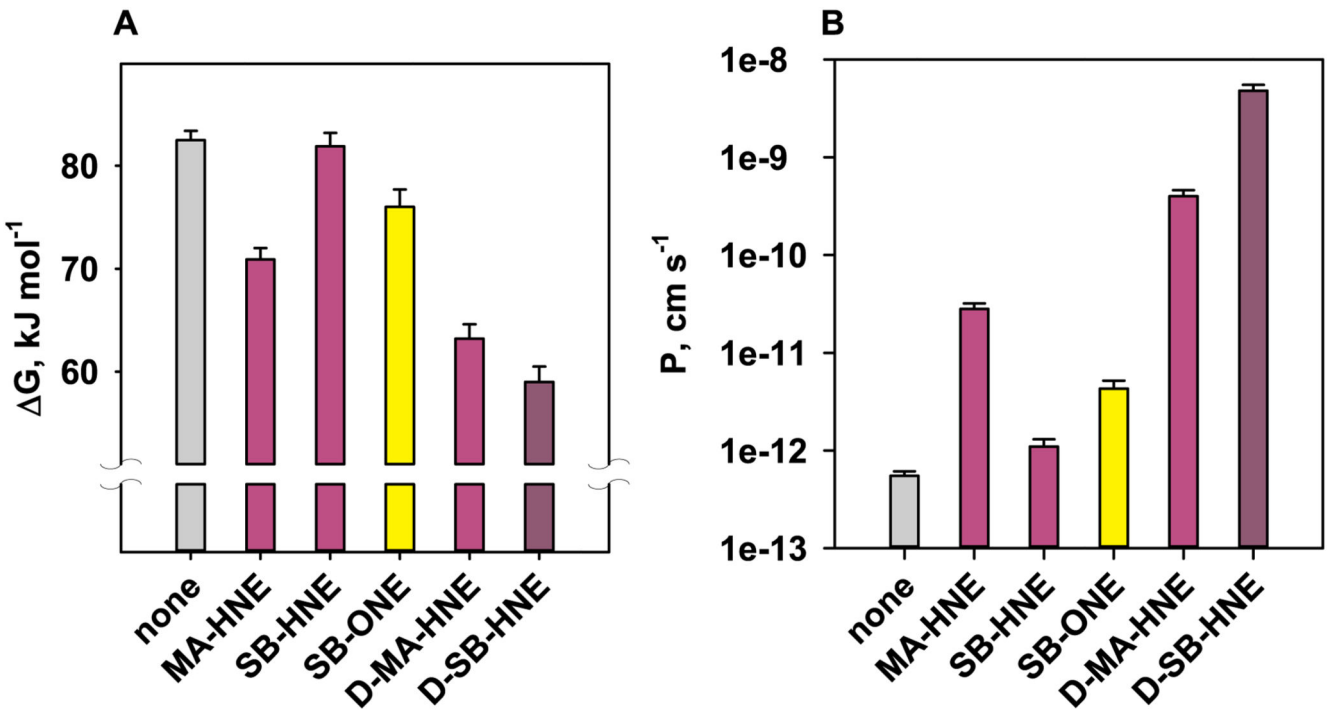

Fig. 6.

Influence of HNE and ONE adducts on free energy barrier (A) and permeability coefficient (B). For labels see Fig. 5.

Europe PMC Funders Author Manuscripts

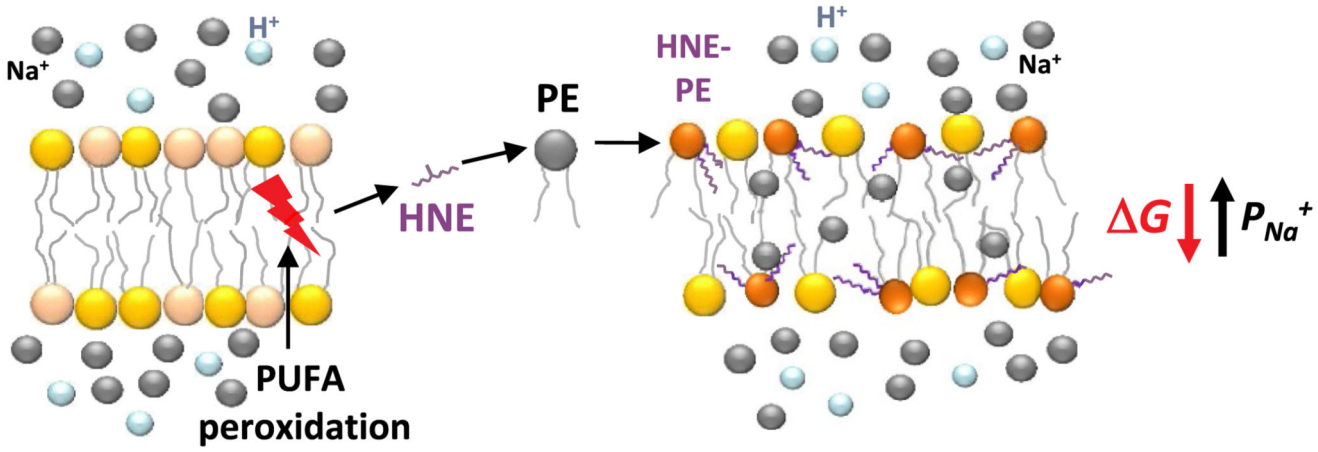

Fig. 7.

Mechanism of 4-hydroxy-2-nonenal (HNE) action on lipid bilayer membrane. HNE, produced by cells under conditions of oxidative stress, covalently modifies phosphatidylethanolamine (PE) forming different HNE-PE adducts (orange-lila). Their position in lipid bilayer membrane is responsible for decrease in energy barrier ΔG and increase in permeability P_{Na} for sodium ions. (For interpretation of the references to colour in this figure legend, the reader is referred to the Web version of this article.)

Europe PMC Funders Author Manuscripts

Europe PMC Funders Author Manuscripts

Table 1

Lipid bilayer compositions used in MD simulations.

Bilayer composition	Name	Number of molecules
DOPC:DOPE	PC:PE	64/64
DOPC:HNE-Michael adduct	MA-HNE	64/64
DOPC:HNE-Schiff base adduct	SB-HNE	64/64
DOPC:ONE-Schiff base adduct	SB-ONE	64/64
DOPC:HNE-double Michael adduct	D-MA-HNE	64/64
DOPC:HNE-double Schiff adduct	D-SB-HNE	64/64